Resonant two-photon ionization spectroscopy of jet-cooled tantalum carbide, TaC

Olha Krechkivska and Michael D. Morse[a)]
Department of Chemistry, University of Utah, Salt Lake City, Utah 84112, USA

(Received 27 May 2010; accepted 23 June 2010; published online 6 August 2010)

The optical spectrum of diatomic TaC has been investigated for the first time, with transitions recorded in the range from 17 850 to 20 000 cm^{-1}. Six bands were rotationally resolved and analyzed to obtain ground and excited state parameters, including band origins, upper and lower state rotational constants and bond lengths, Fermi contact parameter b_F for the ground state, and lambda doubling parameters for the excited states. The ground state of TaC was found to be $X\ ^2\Sigma^+$, originating from the $1\sigma^2 2\sigma^2 1\pi^4 3\sigma^1$ electronic configuration, in which only the valence orbitals arising from the Ta($5d+6s$) and C($2s+2p$) orbitals are listed. All of the rotationally resolved and analyzed bands were found to originate from the ground state, giving $B_0''=0.489\,683(83)$ cm^{-1}, $r_0''=1.749\,01(15)$ Å, and $b_F''=0.131\,20(36)$ cm^{-1} (1σ error limits) for $^{181}Ta\ ^{12}C$. Comparison of the Fermi contact parameter to the atomic value shows that the 3σ orbital is approximately 75% Ta $6s$ in character. The other group 5 transition metal carbides, VC and NbC, have long been known to have $1\sigma^2 2\sigma^2 1\pi^4 1\delta^1$, $^2\Delta$ ground states, with low-lying $1\sigma^2 2\sigma^2 1\pi^4 3\sigma^1$, $^2\Sigma^+$ excited states. The emergence of a different ground state in TaC, as compared to VC and NbC, is due to the relativistic stabilization of the $6s$ orbital in Ta. This lowers the energy of the $6s$-like 3σ orbital in TaC, causing the $1\sigma^2 2\sigma^2 1\pi^4 3\sigma^1$, $^2\Sigma^+$ state to fall below the $1\sigma^2 2\sigma^2 1\pi^4 1\delta^1$, $^2\Delta$ state. © *2010 American Institute of Physics*. [doi:10.1063/1.3464486]

I. INTRODUCTION

Among the transition metal carbides, TaC has the highest melting temperature of 4256 K, and other desirable physical and chemical properties, such as high hardness (1800 kg/mm^2), high elastic modulus (285 GPa), good heat and electric conductivity, and high chemical resistance and catalytic activity.[1,2] These properties suggest a wide range of applications for solid TaC, ranging from hard coatings on mining tools to new materials, including supported thin films,[3] nanoparticles,[4] etc. Despite these attractive properties and wide applications, information on the geometry and electronic configuration of the building blocks of bulk TaC, such as small TaC clusters, including the diatomic molecule, remains very limited. Small TaC clusters, including diatomic TaC, were first isolated in the gas phase and studied by means of Fourier transform mass spectrometry by McElvany *et al.*[5] The formation of small TaC clusters in a supersonic expansion following the reaction of tantalum and acetylene in a laser ablation source was studied by Heaven *et al.*[6]

No spectroscopic studies on diatomic TaC have been previously reported. The first computational study of the potential energy curves and spectroscopic constants of TaC and TaC^+ was performed by Majumdar *et al.*[7] at a variety of different levels of theory. They find the ground state to be $X\ ^2\Sigma^+$, originating from the $1\sigma^2 2\sigma^2 1\pi^4 3\sigma^1$ electronic configuration with a bond length of $r_e=1.799$ Å and a vibrational frequency of 748 cm^{-1}. The ordering of the low-lying excited states changes with the level of theory employed, however. At the CASSCF-SOCI level of theory, the first and second excited states are $^4\Delta$ and $^2\Pi$, lying 0.43 and 0.48 eV above the ground state, respectively.[7] In the course of their study of the Ta_nC_m clusters, Heaven *et al.*[6] performed B3P86 density functional calculations on TaC as well as on the larger clusters. Diatomic TaC was again found to have a $^2\Sigma^+$ ground state with a bond length of 1.76 Å and a vibrational frequency of 977 cm^{-1}. Finally, in a B3LYP density functional investigation of all of the $5d$ transition metal carbides,[8] TaC was again found to have a $^2\Sigma^+$ ground state, originating from the $1\sigma^2 2\sigma^2 1\pi^4 3\sigma^1$ configuration. The bond length was predicted to be 1.735 Å, and the vibrational frequency was calculated to be 944 cm^{-1}. The first excited state was found to be $^4\Delta$, lying only 0.28 eV above the ground state.[8]

An interesting comparison can be made between TaC and other group 5 transition metal carbides. Diatomic VC and NbC have been previously studied, both experimentally and theoretically. Diatomic VC has been investigated by electron spin resonance methods in cryogenic rare gas matrices. Its ground state has been identified as a $^2\Delta_{3/2}$ state, for which the orbital angular momentum is quenched in the cryogenic matrix.[9] A recent computational investigation of VC also predicts a $^2\Delta$ ground state, with $^4\Delta$ and $^2\Sigma^+$ as low-lying excited states, located 0.18 and 0.30 eV above the ground state, respectively.[10] A combined R2PI/LIF and density functional study of diatomic NbC also found its ground state to be $^2\Delta_{3/2}$, originating from the $1\sigma^2 2\sigma^2 1\pi^4 1\delta^1$ configuration.[11] Low-lying excited states of $^2\Sigma^+$ and $^4\Delta$ were computed to lie 0.42 and 0.55 eV above the ground state, respectively.[11] In both VC and NbC, the low-lying $^2\Sigma^+$ and

[a)]Electronic mail: morse@chem.utah.edu. FAX: (801)-581-8433.

$^4\Delta$ states derive from the $1\sigma^2 2\sigma^2 1\pi^4 3\sigma^1$ and $1\sigma^2 2\sigma^1 1\pi^4 3\sigma^1 1\delta^1$ configurations, respectively.

In agreement with the computational studies, the spectroscopic results obtained in the present study demonstrate that the ground state of TaC is $^2\Sigma^+$, deriving from the $1\sigma^2 2\sigma^2 1\pi^4 3\sigma^1$ configuration. The emergence of a different ground state in TaC demonstrates that the relativistic stabilization of the 6*s*-like 3σ molecular orbital lowers the energy of the $^2\Sigma^+$ term, as compared to the $^2\Delta$ and $^4\Delta$ terms, so $^2\Sigma^+$ emerges as the ground state.

II. EXPERIMENTAL

Diatomic TaC was investigated using resonant two-photon ionization (R2PI) spectroscopy. We will not provide a detailed description of the apparatus here, since that has been provided previously.[12] In brief, the R2PI apparatus consists of two chambers that are differentially pumped. The first chamber is pumped by a VHS-10 diffusion pump, backed by a KDH-130 rotary mechanical pump, and consists of a pulsed supersonic nozzle, a disk vaporization assembly, and a molecular beam skimmer (1 cm diameter and 50° inside angle). To produce diatomic metal-ligand molecules, output radiation from a pulsed Nd:YAG laser (532 or 355 nm) is focused onto a metal target disk and is timed to coincide with a pulse of helium carrier gas seeded with ligand gas. In order to vaporize metal uniformly, the metal sample is attached to a mechanism that rotates and translates the sample, so that a spiral pattern is traced out on the sample by the ablation laser. The metal containing plasma that is produced flows down a narrow channel (2 mm diameter $\times$ 1.3 cm long) prior to expansion into the chamber, which is maintained at a pressure of 4×10^{-5} Torr, as read on an ion gauge that was calibrated on air.

The second chamber is pumped by an Edwards 160 diffusion pump, backed by a Welch 1397 rotary mechanical pump, and houses a reflectron-type time-of-flight mass spectrometer (RTOFMS) with Wiley–McLaren ion source optics and a microchannel plate detector.[13,14] The molecular beam is exposed to the output of the Nd-YAG pumped tunable dye laser counterpropagating along the axis of the molecular beam and is crossed at right angles by the output of an ArF excimer laser (193 nm) about 40 ns later in time. Molecules that absorb the dye laser radiation are then ionized by the excimer laser in a resonant two-photon ionization process. The resulting ions are separated by mass in the RTOFMS and detected with the microchannel plate detector. To provide the optical spectrum, the ion signal of the molecule of interest is recorded as a function of the dye laser frequency.

In the past, we have attempted to study diatomic TaC, but these attempts were unsuccessful due to insufficient production of diatomic TaC in the molecular beam. In the present experiment, our first attempt to produce this molecule used a Ta:C sample alloy that had a molar ratio of 9:1, along with pure helium carrier gas. Varying all possible experimental conditions, such as ablation laser energy, backing pressure, nozzle voltage, and duration of the pulse, no trace of TaC was found in the mass spectrum, even though Ta, TaO, and Ta_2 signals were very strong. For our second attempt, a pure Ta metal disk was employed with helium carrier gas that was seeded with 3% CH_4. Again, the same species were present in the molecular beam, with no trace of diatomic TaC. Decreasing the concentration of methane in the carrier gas to 1%, and averaging over 1000 shots to obtain the mass spectrum, a small peak at the mass of TaC became visible. By decreasing the concentration of CH_4 to 0.25%, a strong TaC signal was finally observed. Based on this success with TaC, we believe that using very low concentrations of methane in the helium carrier gas is the key to producing early transition metal carbides, such as LaC and HfC, in the molecular beam.

Conditions used in the present study are: a pure Ta metal target disk, in combination with helium carrier gas seeded with 0.25% methane. The ablation laser used was the third harmonic of the Nd:YAG laser, at 355 nm, 10 mJ/pulse. For ionization, an unfocused excimer laser operating on the ArF mixture (193 nm) was used. A reservoir pressure of 50 psig was found to be optimal for producing diatomic TaC molecules. Spectra were collected for the ^{181}Ta ^{12}C isotopomer (98.92% natural abundance).

To investigate the vibronic spectra of diatomic TaC, the dye laser was scanned in low resolution mode (0.15 cm^{-1}), giving an output energy of 3–10 mJ. To reveal the rotational structure of each vibronic transition, the dye laser output was narrowed using an air-spaced intracavity etalon, which was pressure scanned with sulfur hexafluoride (SF_6). This provided a resolution of about 0.04 cm^{-1} and an output energy of about 1 mJ. During pressure scans the pressure in the dye laser cavity was varied from 30 to 800 torr; this corresponded to scans over a range of about 15 cm^{-1}. For each high resolution spectrum a reference spectrum of I_2 was collected for calibration purpose.[15] As molecules were traveling toward the light source at the beam velocity of helium (1.77×10^5 cm s^{-1}), all line positions were corrected for the Doppler shift experienced by the molecules. This amounted to a small correction of about 0.1 cm^{-1} for all of the lines recorded in this study.

The measured bands were all found to originate from the same lower state, which is assumed to be the ground state. A combined fit of six analyzed bands was performed using the program PGOPHER, a freely available general purpose program for simulating and fitting rotational, vibrational, and electronic spectra.[16]

III. RESULTS

A. Vibronically resolved spectrum of TaC

The vibronically resolved spectrum of TaC was collected between 17 850 and 20 000 cm^{-1} and is presented in Fig. 1. Over the spectral range 18 300–20 000 cm^{-1}, the density of vibronic states is very high, but in the 17 850–18 300 cm^{-1} range it is difficult to pick the transitions out from the noise in the spectrum. A possible explanation for this change is that the combination of the dye laser photon and the ArF excimer laser photon is insufficient to ionize the TaC molecule in the region below 18 300 cm^{-1}. If this is true, it would place the ionization energy of TaC at approximately IE(TaC) $\approx$ 8.68 eV. To establish whether or not this interpretation is

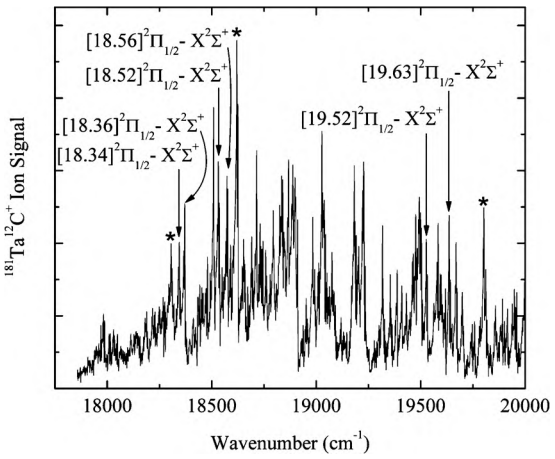

FIG. 1. Vibronically resolved resonant two-photon ionization spectrum of TaC over the range 17 850–20 000 cm^{-1}. The bands labeled with asterisks consist of two or more overlapping transitions.

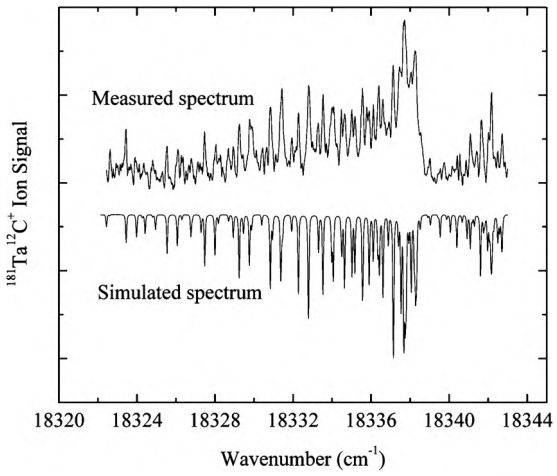

FIG. 2. Rotationally resolved spectrum of the [18.34] $^2\Pi_{1/2}\leftarrow{}^2\Sigma^+$ transition.

correct, it would be necessary to employ a shorter ionization wavelength (perhaps the F_2 excimer laser at 157 nm) as an ionization source and search for vibronic transitions below 18 300 cm^{-1}. An alternative method would be to measure a photoionization efficiency spectrum or to use pulsed field ionization-zero electron kinetic energy spectroscopy to measure the ionization energy precisely, as has been recently done for FeC.[17]

Due to severe vibronic congestion in the low resolution spectrum, and the absence of TaC isotopomers, no definitive vibronic progressions could be identified. It was simply impossible to group the observed vibronic bands into band systems. As a result, all information about the ground and excited states of TaC is obtained from the rotationally resolved spectra. Rotationally resolved spectra of ten bands were collected, and six of these were successfully analyzed and fitted to obtain band origin positions, ground and exited state rotational constants, hyperfine parameters, and lambda doubling parameters. The remaining rotationally resolved bands that were not analyzed appeared to be single bands in the low resolution spectra, but seemed to be overlapping bands when investigated at higher resolution. These unanalyzed bands are identified with asterisks in Fig. 1. All of the rotationally resolved and fitted spectra were found to originate from the same state, which is assumed to be the ground vibronic state of the molecule. This is the X $^2\Sigma^+$ state that is calculated to be the ground state in all of the computational studies on this molecule. The six rotationally resolved bands were analyzed, simultaneously fitted, and simulated using the PGOPHER program to obtain the most accurate ground state parameters.[16] Line positions for all of the rotationally resolved and analyzed bands of TaC have been submitted to the Electronic Physics Auxiliary Publication Service[18] of the American Institute of Physics and are also available from the author (M.D.M.).

B. Rotationally resolved spectra of ^{181}TaC

The rotationally resolved spectra collected in this study for TaC are all qualitatively similar in appearance, as illustrated in Figs. 2–4. In all of the spectra recorded, the band is shaded to the red, with the most intense feature corresponding to a band head. As shown most clearly in Fig. 2, however, the band head appears to be doubled, with the two heads about 0.5 cm^{-1} apart. Additional weaker features occur to the blue of the band head in all bands that were resolved, culminating in a second band head about 4 cm^{-1} to the blue of the most intense band head. This second band head is also doubled, with a similar splitting as in the stronger band head.

These rotationally resolved spectra are too complicated to result from a Hund's case (a)–Hund's case (a) transition with large spin-orbit splitting, as would be expected if the ground state were either the $1\sigma^2 2\sigma^2 1\pi^4 1\delta^1$, $^2\Delta$ state or the $1\sigma^2 2\sigma^1 1\pi^4 3\sigma^1 1\delta^1$, $^4\Delta$ state that are calculated to be low-lying electronic states in the molecule.[7] Thus, we focus on the $1\sigma^2 2\sigma^2 1\pi^4 3\sigma^1$, $^2\Sigma^+$ state as the likely ground state of the molecule. This state is favored by the available *ab initio* calculations[6–8] and is also able to account for the complexity of the observed spectra.

Complex spectra are expected in transitions between a Hund's case (b) $^2\Sigma^+$ ground state and a case (a) $^2\Pi_{1/2}$ or $^2\Pi_{3/2}$ upper state, with four apparent branches.[19] Because the

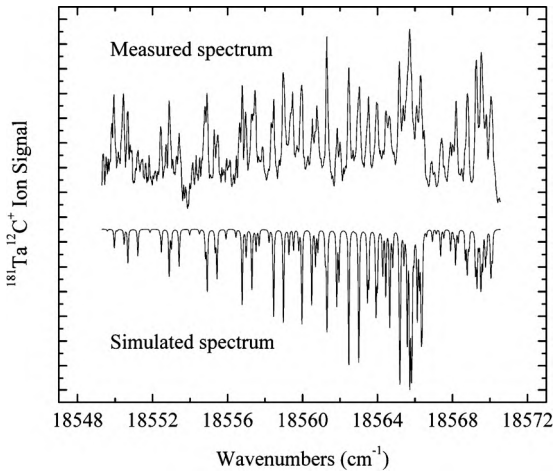

FIG. 3. Rotationally resolved spectrum of the [18.56] $^2\Pi_{1/2}\leftarrow{}^2\Sigma^+$ transition.

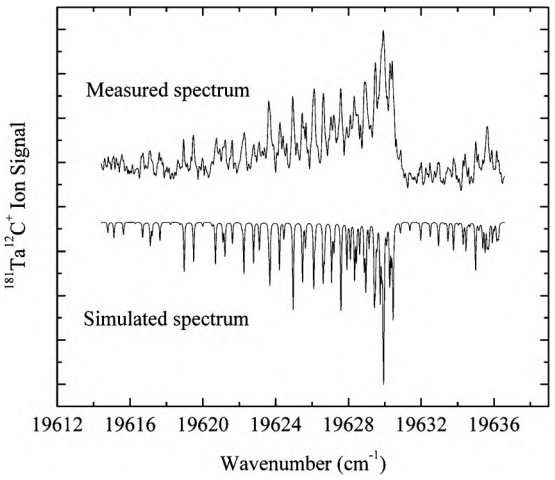

FIG. 4. Rotationally resolved spectrum of the [19.63] $^2\Pi_{1/2} \leftarrow {}^2\Sigma^+$ transition.

pattern-forming quantum numbers in the upper and lower states are J′ and N″, respectively, these four branches correspond to values of J′-N″ of 3/2, 1/2, −1/2, and −3/2. In addition, most of the transition metal molecules that have magnetically active (I>0) nuclei and $^2\Sigma^+$ ground states in which the 3σ orbital is singly occupied, such as ScO,[20,21] YO,[22,23] LaO,[24] LaS,[25] and CoC,[26] belong to Hund's case $b_{\beta S}$.[27] In this coupling case, the magnetic hyperfine interaction $b_F \hat{\boldsymbol{I}} \cdot \hat{\boldsymbol{S}}$ dominates over the spin-rotation interaction $\gamma \hat{\boldsymbol{N}} \cdot \hat{\boldsymbol{S}}$, causing $\boldsymbol{I}$ and $\boldsymbol{S}$ to couple to form the resultant $\boldsymbol{G}$. Finally, $\boldsymbol{G}$ couples with $\boldsymbol{N}$ to form the total angular momentum $\boldsymbol{F}$.[27] The ^{181}Ta nucleus has a large nuclear spin (I =7/2) and a rather large nuclear magnetic moment (2.35 nuclear magnetons),[28] making the $^2\Sigma^+(b_{\beta S})$ coupling case quite likely. For ^{181}TaC, I=7/2, and S=1/2, giving G=3, 4, with a splitting between these levels of $4b_F$. Further, if the 3σ orbital were purely Ta 6s in character, the atomic parameter $b_{F,6s}=0.1750$ cm^{-1} for ^{181}Ta in its $5d^46s^1$ configuration[29] would lead to a splitting between G=3 and 4 of 0.70 cm^{-1}. This is similar in magnitude to the doubling of all the features in the spectrum, where the observed splitting is about 0.5 cm^{-1}.

Leaving aside the question of whether the upper state is $^2\Pi_{1/2}$ or $^2\Pi_{3/2}$, we adopt a modified version of the more commonly occurring $^2\Pi(a)-{}^2\Sigma^+(b_{\beta J})$ branch labeling scheme. In the modified scheme,[24,30,31] the $^2\Pi(a)-{}^2\Sigma^+(b_{\beta J})$ branch labels, specified by $^{\Delta N}\Delta J_{F_i' F_i''}(N'')$, are changed so that the F_i'' label is replaced by the value of G″. Thus, for a $^2\Pi_{1/2}-{}^2\Sigma^+(b_{\beta S})$ system, the eight hyperbranches are $^{O}P_{1G''}$, $^{P}P_{1G''}+{}^{P}Q_{1G''}$, $^{Q}Q_{1G''}+{}^{Q}R_{1G''}$, and $^{R}R_{1G''}$, where G″=3,4. Likewise, for a $^2\Pi_{3/2}-{}^2\Sigma^+(b_{\beta S})$ system, the eight hyperbranches are $^{P}P_{2G''}$, $^{Q}P_{2G''}+{}^{Q}Q_{2G''}$, $^{R}Q_{2G''}+{}^{R}R_{2G''}$, and $^{S}R_{2G''}$, where G″=3,4. The upper states of $^2\Pi_{1/2}$ or $^2\Pi_{3/2}$ may be distinguished by the first lines in the hyperbranches, with first lines (labeled by N″) of $^{O}P_{1G''}(2)$, $^{P}P_{1G''}(1)+{}^{P}Q_{1G''}(1)$, $^{Q}Q_{1G''}(0)+{}^{Q}R_{1G''}(1)$, and $^{R}R_{1G''}(0)$ for $^2\Pi_{1/2} \leftarrow {}^2\Sigma^+$ and $^{P}P_{2G''}(3)$, $^{Q}P_{2G''}(2)+{}^{Q}Q_{2G''}(2)$, $^{R}Q_{2G''}(1)+{}^{R}R_{2G''}(1)$, and $^{S}R_{2G''}(0)$ for $^2\Pi_{1/2} \leftarrow {}^2\Sigma^+$.[19] Thus, a $^2\Pi_{3/2} \leftarrow {}^2\Sigma^+(b_{\beta S})$ transition lacks some of the lines that would be present in a $^2\Pi_{1/2} \leftarrow {}^2\Sigma^+(b_{\beta S})$ transition. An additional distinction between these two types of bands lies in the lambda doubling of the upper $^2\Pi_\Omega$ state. In the case of $^2\Pi_{1/2}$, the lambda doubling is expected to be larger than in the $^2\Pi_{3/2}$ case and to show a magnitude proportional to (J+1/2).[32] In contrast, a $^2\Pi_{3/2}$ state is expected to have a much smaller lambda doubling and a magnitude proportional to $(J-1/2)(J+1/2)\times(J+3/2)$.[32] Thus, in the case of $^2\Pi_{3/2}$, the lambda doubling is expected to be unobservable in the low-J lines that are populated in our experiment, but to rapidly grow in magnitude as J increases.

None of the six rotationally analyzed bands could be fitted to the expected structure of a $^2\Pi_{3/2}$ upper state, but all could be explained as having $^2\Pi_{1/2}$ upper states. It was necessary to include lambda doubling in the upper state in order to fit the bands, but the splitting pattern expected for the $^2\Pi_{3/2}$ state was not in good agreement with the measured line positions. In addition, for many of the bands, lines were observed that do not occur for a $^2\Pi_{3/2} \leftarrow {}^2\Sigma^+$ transition. Thus, we are confident that all of the upper states observed correspond to states with Ω=1/2. It is likely that these upper states are severely mixed by spin-orbit interaction so that S, Λ, and Σ may be poorly defined, but all are consistent only with Ω=1/2. Thus, upper states that are primarily $^4\Pi_{1/2}$, $^4\Pi_{-1/2}$, or $^4\Delta_{1/2}$ in character are also candidates for the upper states.

Hyperfine splitting arising in the upper states was not resolved. Likewise, the splitting of the G″=3 or 4 sublevels into the various F″ components was not resolved either. The bands could all be explained by including the splitting into G″-levels in the lower state and the lambda doubling in the upper state. The spin-rotation interaction could be ignored in the lower state, and the hyperfine interaction could be ignored in the upper state. The bands were therefore fitted to the $\hat{N}^2$ form of the rotational Hamiltonian given by

$$\hat{H} = B\hat{N}^2 + b_F \hat{\boldsymbol{I}} \cdot \hat{\boldsymbol{S}} \tag{3.1}$$

for the ground $^2\Sigma^+$ state and

$$\hat{H} = T_0 + B\hat{N}^2 + A\hat{L}_z\hat{S}_z + \tfrac{1}{2}(p+2q) \times (e^{-2i\varphi}\hat{J}_+\hat{S}_+ + e^{+2i\varphi}\hat{J}_-\hat{S}_-) \tag{3.2}$$

for the excited $^2\Pi_{1/2}$ states.

The simulation and fitting of the bands was performed using PGOPHER, with all six bands fitted simultaneously in order to decrease the uncertainty in the ground state constants.[16] Despite the complexity of the bands, the fact that all can be fitted with the same ground state constants makes us confident that the assignments are correct. Using this procedure, accurate values of B_0'' and b_F'' have been determined for the ground state, and B′ and (p′+2q′) have been determined for each of the upper states that were analyzed. For this system, the spin-orbit splitting A of the upper $^2\Pi$ states has not been determined and is expected to be very large. Therefore, A was set to 2000 cm^{-1} in all of our upper states, so that spin-uncoupling interactions between the Ω=1/2 and 3/2 components of the $^2\Pi$ states were inconsequential in the

TABLE I. Ground and excited state spectroscopic constants of ^{181}Ta ^{12}C. Error limits (1σ) in the fitted parameters are provided in parentheses in units of the last digit quoted.

	X $^2\Sigma^+$	[18.34] $^2\Pi_{1/2}$	[18.36] $^2\Pi_{1/2}$	[18.52] $^2\Pi_{1/2}$	[18.56] $^2\Pi_{1/2}$	[19.52] $^2\Pi_{1/2}$	[19.63] $^2\Pi_{1/2}$
ν_0(cm^{-1}) [a]		19 336.7865(25)	19 362.8770(32)	19 523.3372(31)	19 564.7614(24)	20 519.5936(24)	20 628.9787(27)
B (cm^{-1})	0.489683(83)	0.407309(87)	0.413147(98)	0.40400(12)	0.403566(82)	0.402641(80)	0.417110(88)
R (Å)	1.74901(15)	1.91774(20)	1.90414(23)	1.92557(29)	1.92661(20)	1.92882(19)	1.89507(20)
b_F (cm^{-1})	0.13120(36)						
p+2q (cm^{-1})		0.07362(50)	0.01533(68)	0.05381(76)	0.14588(43)	0.08664(50)	−0.02253(61)

[a]All spectra were fitted using a large spin-orbit parameter, A=2000 cm^{-1}, in the upper state. Therefore, the fitted band origins are shifted 1000 cm^{-1} to higher energies from the subband origins.

fits. As a result, the reported values of T_0 are 1000 cm^{-1} higher than the approximate subband origins. Nevertheless, we report our values in this format so that other investigators can reproduce the simulated bands using PGOPHER, if they so desire.

Line positions for all of the rotationally analyzed bands of TaC have been deposited with the Electronic Physics Auxiliary Publication Service of the American Institute of Physics[18] and are also available from the author (M.D.M.). The electronic document also contains measured and simulated spectra for all of the rotationally resolved bands. The spectroscopic constants resulting from the simultaneous fit of all six bands are provided in Table I, along with the vibrationally averaged bond lengths that are obtained from simple inversion of the fitted B values. The simulated spectra displayed in Figs. 2–4 were all calculated assuming a temperature of 33 K for the jet-cooled TaC molecules. Although this is a bit warmer than we find for many of our spectra, it seems to reproduce the measured spectra reasonably well.

IV. DISCUSSION

This work has determined that the ground state of TaC is $1\sigma^2 2\sigma^2 1\pi^4 3\sigma^1$, $^2\Sigma^+$. A qualitative molecular orbital diagram is displayed in Fig. 5 to provide a basis for discussion of the bonding in this molecule. In this diagram, the 1σ orbital of TaC is assumed to be mainly $2s$ carbon in character, although some mixing with the C $2p\sigma$ and Ta $5d\sigma$ orbitals is possible. The 2σ and 4σ orbitals are the bonding and antibonding combinations of the Ta $5d\sigma$ and C $2p\sigma$ orbitals. The 1π and 2π orbitals are the analogous bonding and antibonding combinations of the Ta $5d\pi$ and C $2p\pi$ orbitals. The 1δ orbitals are almost entirely Ta $5d\delta$ in character and are nonbonding

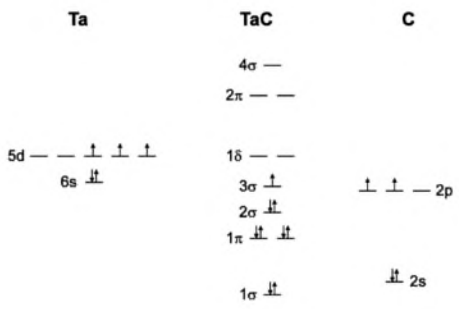

FIG. 5. Qualitative molecular orbital diagram of TaC.

due to the lack of orbitals of δ symmetry on carbon. The 3σ orbital is also expected to be nonbonding and mainly Ta $6s$ in character. This is confirmed by our hyperfine measurements, which provide b_F=0.13120(36) cm^{-1}, which compares to the value $b_{F,6s}$=0.1750 cm^{-1} for ^{181}Ta in its $5d^4 6s$ configuration, as provided by Büttgenbach.[29] Comparison of the b_F values for TaC and atomic Ta shows that the 3σ orbital of TaC is roughly 75% Ta $6s$ in character.

The high proportion of metal ns character in the 3σ orbital of TaC is in agreement with hyperfine measurements in related metal carbides. Among the $3d$ series of transition metal carbides, hyperfine measurements on CoC demonstrate that the 3σ orbital has 89% Co $4s$ character.[26] In the $4d$ carbides, hyperfine studies show that this orbital has 71% $5s$ character in ZrC,[33] 83% $5s$ character in RuC,[34] and 69% $5s$ character in RhC.[35] The only other member of the $5d$ series for which hyperfine measurements are available is OsC, for which the 3σ orbital has 84%–95% $6s$ character.[36] These results show that the 3σ orbital is dominated by metal ns character across the entire range of the transition metal carbides. Diatomic TaC is apparently no different from other transition metal carbides in this regard.

This result contrasts with the results of an *ab initio* calculation on TaC, in which the Mulliken population in the Ta $5s+6s$ orbitals for the X $^2\Sigma^+$ ground state is found to be 4.000.[7] This implies that there is no unpaired electron density in the tantalum $6s$ orbital, in disagreement with our result. We have considered whether there might be some alternative interpretation of our measurements that could bring theory and experiment into agreement, but this does not seem to be the case. In particular, ^{181}Ta has a large electric quadrupole moment of $+3\times10^{-24}$ cm^2,[28] and an e^2Qq_0 value of −0.1072 cm^{-1} has been found in the related molecule, TaO X $^2\Delta_{3/2}$.[37] Simulation of the TaC spectrum with significant quadrupole moments included, however, leads to much more complicated spectra. The simple splitting of the ground state levels into G″=3 and G″=4 sublevels only occurs when the hyperfine interaction is dominated by the Fermi contact term. Accordingly, we are convinced that our hyperfine analysis is correct, and that the singly occupied 3σ orbital in the TaC X $^2\Sigma^+$ state is dominated by tantalum $6s$ character.

In contrast to the hyperfine measurement, the measured value of the ground state bond length, r_0=1.749 Å, is in fairly good agreement with the calculated values of r_e =1.76,[6] 1.799,[7] and 1.735 Å.[8]

Diatomic TaC differs significantly from its congeners, VC and NbC, in having a ground state of $1\sigma^2 2\sigma^2 1\pi^4 3\sigma^1$,

TABLE II. Measures of the orbital energy difference $\varepsilon(s)-\varepsilon(d)$ in group 5 atoms.

	$\varepsilon(s)-\varepsilon(d)$ (eV)		
Method[a]	V	Nb	Ta
$E(d^3s^2,{}^4F_{3/2})-E(d^4s^1,{}^6D_{1/2})$	−0.262	+0.142	−1.210
$E(d^3s^1,{}^5F_1,M^+)-E(d^4,{}^5D_0,M^+)$	0.323	0.292	−1.562

[a]See text for description. Atomic energy levels taken from Ref. 38.

$^2\Sigma^+$, rather than $1\sigma^2 2\sigma^2 1\pi^4 1\delta^1$, $^2\Delta$. This change in ground configuration results from the change in atomic orbital energies as one moves down the column of group 5 elements from V to Nb to Ta. The relevant atomic energy level data are provided in Table II. Using known atomic energy levels,[38] the energy difference between the (n+1)*s* and n*d* orbitals, $\varepsilon(s)-\varepsilon(d)$, may be estimated by either of two methods. In the first method, $\varepsilon(s)-\varepsilon(d)$ is estimated as $E(d^3s^2,{}^4F_{3/2})-E(d^4s^1,{}^6D_{1/2})$. This method utilizes data from the energy levels of the neutral atom and measures the amount of energy required to excite the atom from the lowest level of the d^4s^1 configuration to the lowest level of the d^3s^2 configuration, which is negative in the cases of V and Ta. Alternatively, $\varepsilon(s)-\varepsilon(d)$ can be estimated as the difference between the energy required to remove a *d* electron and that required to remove an *s* electron from the d^4s^1, $^6D_{1/2}$ level of the neutral atom. This energy difference is equivalent to the difference in energy between the d^3s^1, $^5F_1$ and d^4, $^5D_0$ levels of the atomic cation, which may be designated as $E(d^3s^1,{}^5F_1,M^+)-E(d^4,{}^5D_0,M^+)$. Other measures of the difference in orbital energies could be devised, but these two methods are sufficient for our purposes. The data displayed in Table II show that while the valence *s* and *d* orbitals are similar in energy in V and Nb, the 6*s* orbital lies more than 1 eV below the 5*d* orbital in Ta. It is this dramatic stabilization in the 6*s* orbital that causes $1\sigma^2 2\sigma^2 1\pi^4 3\sigma^1$, $^2\Sigma^+$ to emerge as the ground state of TaC.

A change in electronic configuration similar to that found here also occurs as one moves from the 4*d* metal carbide to the 5*d* metal carbide in other columns of the periodic table. For example, the ground term of MoC is $1\sigma^2 2\sigma^2 1\pi^4 1\delta^2$, $^3\Sigma^-$,[39] while that of WC is $1\sigma^2 2\sigma^2 1\pi^4 1\delta^1 3\sigma^1$, $^3\Delta_1$.[40] Likewise, the ground term of RuC is $1\sigma^2 2\sigma^2 1\pi^4 1\delta^4$, $^1\Sigma^+$,[34] while that of OsC is $1\sigma^2 2\sigma^2 1\pi^4 1\delta^3 3\sigma^1$, $^3\Delta_3$.[36] Among the group 9 metal carbides, RhC has a ground term of $1\sigma^2 2\sigma^2 1\pi^4 1\delta^4 3\sigma^1$, $^2\Sigma^+$,[35,41] while the ground term of IrC is $1\sigma^2 2\sigma^2 1\pi^4 1\delta^3 3\sigma^2$, $^2\Delta_{5/2}$.[42] In all of these examples, it is the stabilization of the 6*s* orbital relative to the 5*d* orbitals that lowers the energy of the 3σ orbital relative to the 1δ orbitals, causing a different ground state to emerge.

The stabilization of the 6*s* orbital relative to the 5*d* orbital is primarily a relativistic effect, as illustrated in Table III, which compares the orbital energies obtained in a nonrelativistic numerical Hartree–Fock calculation to those obtained in a relativistic numerical Dirac–Fock calculation.[43] As is well-known,[44,45] relativistic effects stabilize the *s* orbitals due to their penetration close to the nucleus, where in a classical picture the kinetic energy and electron velocity become very large. The high velocity of the *s* electrons when they are close to the nucleus causes them to be the most affected by relativistic effects. The mass-velocity effect thus causes the *s* orbital to contract and drop in energy. Simultaneously, the nonpenetrating *d* orbitals are shielded from the nuclear charge more effectively following the relativistic *s* orbital contraction, causing them to expand and move higher in energy. The effect in Ta is quite dramatic, lowering the energy of the 6*s* orbital by 15.6% while raising the 5*d* orbital energy by 15%–20%, depending on how the orbital angular momentum ℓ is coupled to the electron spin *s*. It is the combination of the stabilization of the 6*s* orbital and the destabilization of the 5*d* orbitals that causes the ground states of the 5*d* metal carbides often to differ from that of their 3*d* and 4*d* congeners.

TABLE III. Relativistic effects on atomic orbital energies. The values provided give the percentage change in orbital energy when relativistic effects are included, as compared to the nonrelativistic treatment. Relativistic results are from numerical Dirac–Fock calculations; nonrelativistic results are from a numerical Hartree–Fock calculation (Ref. 43). Results are presented separately for the j=5/2 and j=3/2 coupling of the electronic orbital angular momentum ℓ with the electron spin *s* for the n*d* electrons because the spin-orbit interaction causes a significant difference in their energies.

Atom and configuration	$nd_{5/2}$ orbital (%)	$nd_{3/2}$ orbital (%)	(n+1)*s* orbital (%)
V $3d^34s^2$	+2.34	+1.87	−0.926
Nb $4d^45s^1$	+5.74	+3.78	−5.41
Ta $5d^36s^2$	+20.15	+15.1	−15.60

Table IV presents the ground state electronic configuration and term and the measured bond length for all of the experimentally known transition metal monocarbides. When no experimental data exist, computational results are provided. As expected, the contraction of the n*d* and (n+1)*s* orbitals as one moves across the periodic table generally causes the bond lengths of the transition metal carbides to shorten. A few exceptions to this general trend occur, however. Exceptions occur between the pairs CrC/MnC, CoC/NiC, MoC/TcC, RuC/RhC, RhC/PdC, and OsC/IrC. In all of these cases, the disruption of the trend of shortening bond lengths is correlated with an increase in the number of electrons in the n*s*-like 3σ orbital. Occupation of the nominally nonbonding 3σ orbital clearly causes the bond to lengthen. In essence, occupation of the more diffuse n*s*-like 3σ orbital prevents the atoms from approaching each other as closely. This is likely a Pauli repulsion effect that is mitigated by polarization of the 3σ orbital away from the carbon atom via metal n*s*-n*p* mixing.

V. CONCLUSION

The electronic spectrum of diatomic TaC was recorded in the range from 17 850 to 20 000 cm^{-1}, using resonant two-photon spectroscopy. It is found that the ground state of TaC is a $^2\Sigma^+$ term that originates from the $1\sigma^2 2\sigma^2 1\pi^4 3\sigma^1$ configuration. Measured spectroscopic constants for

TABLE IV. Ground states and bond lengths of transition metal carbides.

3*d* metal carbide	4*d* metal carbides	5*d* metal carbides
ScC (theory)	YC	LaC
$1\sigma^2 1\pi^3 2\sigma^2$, $^2\Pi_{3/2}$	$1\sigma^2 1\pi^3 2\sigma^1 3\sigma^1$, $^4\Pi_{5/2}$	$1\sigma^2 1\pi^4 2\sigma^1$, $^2\Sigma^+$
1.988 Å (r_e)	2.051 Å (r_0)	2.030 Å
Reference 46	Reference 47	Reference 8
TiC (theory)	ZrC	HfC (theory)
$1\sigma^2 1\pi^4 2\sigma^1 3\sigma^1$, $^3\Sigma^+$	$1\sigma^2 1\pi^4 2\sigma^1 3\sigma^1$, $^3\Sigma^+$	$1\sigma^2 1\pi^4 2\sigma^1 3\sigma^1$, $^3\Sigma^+$
1.712 Å (r_e)	1.807 Å (r_0)	1.800 Å (r_e)
Reference 48	Reference 33	Reference 8
VC (theory)	NbC	TaC
$1\sigma^2 1\pi^4 2\sigma^2 1\delta^1$, $^2\Delta_{3/2}$	$1\sigma^2 1\pi^4 2\sigma^2 1\delta^1$, $^2\Delta_{3/2}$	$1\sigma^2 1\pi^4 2\sigma^2 3\sigma^1$, $^2\Sigma^+$
1.636 Å (r_e)	1.700 Å (r_0)	1.749 Å (r_0)
Reference 10	Reference 11	This work
CrC	MoC	WC
$1\sigma^2 1\pi^4 2\sigma^2 1\delta^2$, $^3\Sigma^-$	$1\sigma^2 1\pi^4 2\sigma^2 1\delta^2$, $^3\Sigma^-$	$1\sigma^2 1\pi^4 2\sigma^2 1\delta^1 3\sigma^1$, $^3\Delta_1$
1.619 Å (r_0)	1.676 Å (r_0)	1.714 Å (r_0)
Reference 49	Reference 39	Reference 40
MnC (theory)	TcC (theory)	ReC (theory)
$1\sigma^2 1\pi^4 2\sigma^2 1\delta^2 3\sigma^1$, $^4\Sigma^-$	$1\sigma^2 1\pi^4 2\sigma^2 1\delta^2 3\sigma^1$, $^4\Sigma^-$	$1\sigma^2 1\pi^4 2\sigma^2 1\delta^2 3\sigma^1$, $^4\Sigma^-$
1.640 Å (r_e)	1.710 Å (r_e)	1.692 Å (r_e)
Reference 50	Reference 51	Reference 8
FeC	RuC	OsC
$1\sigma^2 1\pi^4 2\sigma^2 1\delta^3 3\sigma^1$, $^3\Delta_3$	$1\sigma^2 1\pi^4 2\sigma^2 1\delta^4$, $^1\Sigma^+$	$1\sigma^2 1\pi^4 2\sigma^2 1\delta^3 3\sigma^1$, $^3\Delta_3$
1.596 Å (r_0)	1.608 Å (r_0)	1.673 Å (r_0)
References 52 and 53	Reference 34	Reference 36
CoC	RhC	IrC
$1\sigma^2 1\pi^4 2\sigma^2 1\delta^4 3\sigma^1$, $^2\Sigma^+$	$1\sigma^2 1\pi^4 2\sigma^2 1\delta^4 3\sigma^1$, $^2\Sigma^+$	$1\sigma^2 1\pi^4 2\sigma^2 1\delta^3 3\sigma^2$, $^2\Delta_{5/2}$
1.561 Å (r_0)	1.616 Å (r_0)	1.686 Å (r_0)
References 26 and 54	Reference 55	Reference 56
NiC	PdC	PtC
$1\sigma^2 1\pi^4 2\sigma^2 1\delta^4 3\sigma^2$, $^1\Sigma^+$	$1\sigma^2 1\pi^4 2\sigma^2 1\delta^4 3\sigma^2$, $^1\Sigma^+$	$1\sigma^2 1\pi^4 2\sigma^2 1\delta^4 3\sigma^2$, $^1\Sigma^+$
1.631 Å (r_0)	1.712 Å (r_0)	1.677 Å
References 54 and 57	Reference 58	Reference 59

the ground state are $B_0''=0.489\,683(83)$ cm^{-1}, $r_0''=1.749\,014(148)$ Å, and $b_F''=0.131\,20(36)$ cm^{-1} (1σ error limits) for the ^{181}Ta ^{12}C isotopomer. These results are contrasted with the ground states of the congeneric molecules VC and NbC, and it is argued that the difference in the ground configuration and term of TaC results from the relativistic stabilization of the 6*s* orbital in atomic Ta.

ACKNOWLEDGMENTS

The authors thank the U.S. Department of Energy for support of this research under Grant No. DE-FG03-01ER15176.

[1] A. T. Santhanam. in *The Chemistry of Transition Metal Carbides and Nitrides*. edited by S. T. Oyama (Blackie Academic & Professional. London. 1996). pp. 28–52.
[2] N. I. Ilchenko and Y. I. Pyatnitsky. in *Chemistry of Transition Metal Carbides and Nitrides*. edited by S. T. Oyama (Blackie Academic & Professional. London. 1996). pp. 311–326.
[3] R. Teghil. A. De Bonis. A. Galasso. P. Villani. and A. Santagata. Appl. Surf. Sci. **254**. 1220 (2007).
[4] A. Fukunaga. S. Chu. and M. E. McHenry. J. Mater. Sci. Lett. **18**. 431 (1999).
[5] S. W. McElvany and C. J. Cassady. J. Phys. Chem. **94**. 2057 (1990).
[6] M. W. Heaven. G. M. Stewart. M. A. Buntine. and G. F. Metha. J. Phys. Chem. A **104**. 3308 (2000).
[7] D. Majumdar and K. Balasubramanian. Chem. Phys. Lett. **284**. 273 (1998).
[8] J. Wang. X. Sun. and Z. Wu. J. Cluster Sci. **18**. 333 (2007).
[9] Y. M. Hamrick and W. Weltner. Jr.. J. Chem. Phys. **94**. 3371 (1991).
[10] A. Kalemos. T. H. Dunning. Jr.. and A. Mavridis. J. Chem. Phys. **123**. 014301 (2005).
[11] B. Simard. P. I. Presunka. H. P. Loock. A. Bérces. and O. Launila. J. Chem. Phys. **107**. 307 (1997).
[12] D. J. Brugh and M. D. Morse. J. Chem. Phys. **107**. 9772 (1997).
[13] W. C. Wiley and I. H. McLaren. Rev. Sci. Instrum. **26**. 1150 (1955).
[14] B. A. Mamyrin. V. I. Karataev. D. V. Shmikk. and V. A. Zagulin. Zh. Eksp. Teor. Fiz. **64**. 82 (1973).
[15] S. Gerstenkorn and P. Luc. *Atlas du Spectre d'Absorption de la Molécule d'Iode Entre* 14.800–20.000 cm^{-1} (CNRS. Paris. 1978).
[16] C. M. Western. PGOPHER. a Program for Simulating Rotational Structure. University of Bristol. http://pgopher.chm.bris.ac.uk.
[17] Y. C. Chang. C. S. Lam. B. Reed. K. C. Lau. H. T. Liou. and C. Y. Ng. J. Phys. Chem. A **113**. 4242 (2009).
[18] See supplementary material at http://dx.doi.org/10.1063/1.3464486 for 13 pages of line positions. rotational fits. and rotationally resolved spectra of TaC.
[19] G. Herzberg. in *Molecular Spectra and Molecular Structure I. Spectra of Diatomic Molecules*. 2nd ed. (Van Nostrand Reinhold. New York. 1950).
[20] A. Adams. W. Klemperer. and T. M. Dunn. Can. J. Phys. **46**. 2213 (1968).
[21] R. Stringat. C. Athenour. and J. L. Femenias. Can. J. Phys. **50**. 395 (1972).
[22] T. C. Steimle and Y. Al-Ramadin. J. Mol. Spectrosc. **122**. 103 (1987).
[23] T. C. Steimle and J. E. Shirley. J. Chem. Phys. **92**. 3292 (1990).
[24] T. C. Steimle and W. Virgo. J. Chem. Phys. **116**. 6012 (2002).
[25] S. G. He. W. S. Tam. J. W. H. Leung. and A. S. C. Cheung. J. Chem. Phys. **117**. 5764 (2002).
[26] M. Barnes. A. J. Merer. and G. F. Metha. J. Chem. Phys. **103**. 8360 (1995).
[27] T. M. Dunn. in *Molecular Spectroscopy: Modern Research*. edited by K. N. Rao and C. W. Mathews (Academic. New York. 1972). pp. 231–257.
[28] W. Weltner. Jr.. *Magnetic Atoms and Molecules* (Dover. New York. 1983).
[29] S. Büttgenbach. *Hyperfine Structure in 4d- and 5d-Shell Atoms* (Springer-Verlag. Berlin. Heidelberg. 1982).
[30] W. J. Childs and T. C. Steimle. J. Chem. Phys. **88**. 6168 (1988).
[31] J. Shirley. C. Scurlock. and T. Steimle. J. Chem. Phys. **93**. 1568 (1990).
[32] J. M. Brown and A. J. Merer. J. Mol. Spectrosc. **74**. 488 (1979).
[33] S. J. Rixon. P. K. Chowdhury. and A. J. Merer. J. Mol. Spectrosc. **228**. 554 (2004).
[34] J. D. Langenberg. R. S. DaBell. L. Shao. D. Dreessen. and M. D. Morse. J. Chem. Phys. **109**. 7863 (1998).
[35] J. M. Brom. Jr.. W. R. M. Graham. and W. Weltner. Jr.. J. Chem. Phys. **57**. 4116 (1972).
[36] O. Krechkivska and M. D. Morse. J. Chem. Phys. **128**. 084314 (2008).
[37] K. J. Manke. T. R. Vervoort. K. T. Kuwata. and T. D. Varberg. J. Chem. Phys. **128**. 104302 (2008).
[38] C. E. Moore. *Atomic Energy Levels*. Natl. Bur. Stand. U.S. Circ. No. 467 (U. S. Government Printing Office. Washington. D.C.. 1971).
[39] D. J. Brugh. T. J. Ronningen. and M. D. Morse. J. Chem. Phys. **109**. 7851 (1998).
[40] S. M. Sickafoose. A. W. Smith. and M. D. Morse. J. Chem. Phys. **116**. 993 (2002).
[41] A. Lagerqvist and R. Scullman. Ark. Fys. **32**. 475 (1966).
[42] K. Jansson. R. Scullman. and B. Yttermo. Chem. Phys. Lett. **4**. 188 (1969).
[43] J. P. Desclaux. At. Data Nucl. Data Tables **12**. 311 (1973).
[44] P. Pyykko and J. P. Desclaux. Acc. Chem. Res. **12**. 276 (1979).
[45] K. Balasubramanian. J. Phys. Chem. **93**. 6585 (1989).
[46] A. Kalemos. A. Mavridis. and J. F. Harrison. J. Phys. Chem. A **105**. 755 (2001).
[47] B. Simard. P. A. Hackett. and W. J. Balfour. Chem. Phys. Lett. **230**. 103 (1994).
[48] A. Kalemos and A. Mavridis. J. Phys. Chem. A **106**. 3905 (2002).
[49] D. J. Brugh. M. D. Morse. A. Kalemos. and A. Mavridis. J. Chem. Phys.

133. 034303 (2010).
[50] A. Kalemos, T. H. Dunning, Jr., and A. Mavridis, J. Chem. Phys. **124**, 154308 (2006).
[51] P. Jackson, G. E. Gadd, D. W. Mackey, H. van der Wall, and G. D. Willett, J. Phys. Chem. A **102**, 8941 (1998).
[52] W. J. Balfour, J. Cao, C. V. V. Prasad, and C. X. Qian, J. Chem. Phys. **103**, 4046 (1995).
[53] M. D. Allen, T. C. Pesch, and L. M. Ziurys, Astrophys. J. **472**, L57 (1996).
[54] M. A. Brewster and L. M. Ziurys, Astrophys. J. **559**, L163 (2001).
[55] W. J. Balfour, S. G. Fougère, R. F. Heuff, C. X. W. Qian, and C. Zhou, J. Mol. Spectrosc. **198**, 393 (1999).
[56] A. J. Marr, M. E. Flores, and T. C. Steimle, J. Chem. Phys. **104**, 8183 (1996).
[57] D. J. Brugh and M. D. Morse, J. Chem. Phys. **117**, 10703 (2002).
[58] J. D. Langenberg, L. Shao, and M. D. Morse, J. Chem. Phys. **111**, 4077 (1999).
[59] T. C. Steimle, K. Y. Jung, and B.-Z. Li, J. Chem. Phys. **102**, 5937 (1995).